


Molecular Mott state in the deficient spinel GaV₄S₈Heung-Sik Kim ^{1,2}, Kristjan Haule,¹ and David Vanderbilt¹¹*Department of Physics and Astronomy, Rutgers University, Piscataway, New Jersey 08854-8019, USA*²*Department of Physics, Kangwon National University, Chuncheon 24341, Korea* (Received 22 October 2018; revised 24 February 2020; accepted 24 July 2020; published 6 August 2020)

In this study, we investigated theoretically the Mott-insulating phase of a deficient spinel chalcogenide GaV₄S₈, which is known to form a tetrahedral V₄S₄ cluster unit that results in molecular orbitals (MOs) with a narrow bandwidth in the noninteracting limit. We used a cluster extension of charge self-consistent embedded dynamical mean-field theory to study the impact of strong intracluster correlations on the spectral properties as well as the structural degrees of freedom of the system. We found that the strong tetrahedral clustering renders the atomic Mott picture ineffective, and that the resulting MO picture is essential to describe the Mott phase. It was also found that, while the spectral properties can be qualitatively described by the truncation of the Hilbert space down to the lowest-energy MO, a proper description of the structural degrees of freedom requires the inclusion of multi-MO correlations that span a larger energy window. Specifically, we found that the lowest-energy MO description overemphasizes the clustering tendency, while the inclusion of the Hund's coupling between the lower- and higher-energy MOs corrects this tendency, bringing the theoretically predicted crystal structure into good agreement with the experiment.

DOI: [10.1103/PhysRevB.102.081105](https://doi.org/10.1103/PhysRevB.102.081105)

Introduction. Intermetallic covalency in transition-metal chalcogenides or oxides often leads to the formation of density waves or transition-metal clustering [1]. While this typically results in a reduction of Fermi surface, more dramatic changes may happen in correlated systems such as VO₂ [2–5] or 1T phases of TaS₂ and NbSe₂ [6–10]. Another interesting class of materials is ternary deficient spinel chalcogenides AM₄X₈ (A = Al, Ga, Ge; M = Ti, V, Nb, Mo, Ta; X = S, Se), where the four M sites form a tetrahedral cluster and drive the system to be Mott insulating [11–19]. Among this family, GaV₄S₈ has been actively studied recently because of the existence of a rhombohedral polar (i.e., with nonzero bulk electric polarization) phase with significant magnetoelectric coupling and the formation of a skyrmion crystal below T_C = 13 K [20–22]. Based on this observation and the strong V₄ clustering, this system has been suggested to be a Mott insulator with the V₄ molecular orbitals (MOs) comprising the correlated subspace. It seems likely that, as in the example of VO₂, the electron-lattice coupling in GaV₄S₈ can be modified by electron correlations in a nontrivial manner, which may affect the nature of the low-temperature multiferroic phase [20–22].

Dynamical mean-field theory (DMFT) has become a standard tool for tackling such correlated materials in an *ab initio* manner [23–25]. The cluster extension of the conventional single-site DMFT [24,26] can be used to systematically increase the range of spatial correlations, extending the notion of locality from an atomic site to a cluster. However, the exponential scaling of the computational cost becomes an issue at this point; the number of cubic t_{2g} orbitals in the V₄ cluster is 12, and directly tackling such problem is extremely challenging even with the use of the most state-of-the-art

impurity solvers such as continuous-time Monte Carlo [27–29]. Because of this difficulty, a proper *ab initio* study of the Mott phase of GaV₄S₈, fully incorporating lattice and charge degrees of freedom, has not yet appeared.

Hence, in this study, we have studied the Mott phase of GaV₄S₈ in the high-temperature cubic (nonpolar) phase above T = 45 K, specifically focusing on the occurrence of the Mott phase via the MO formation and its impact on the structural degrees of freedom. We employed fully charge self-consistent DMFT with cluster MO bases applied to the tetrahedral cluster of four V sites, starting from the simplest model containing only the lowest-energy MO (T² in Fig. 1) and progressively enlarging the correlated Hilbert space to include the majority of t_{2g} states in the V₄ cluster (T² + E + T_a¹). Our cluster MO-DMFT prediction was compared to most standard as well as advanced density functional theory (DFT) exchange-correlation functionals, including SCAN meta-GGA [30] and Heyd-Scuseria-Ernzerhof (HSE) hybrid functionals [31,32]. While these all fail to predict an insulating phase, our cluster calculation opens a gap very naturally, thus demonstrating that the MO picture is essential for describing the Mott phase. Surprisingly, the V₄S₄ clustering is strongly affected by the strength of the Hund's coupling at the V sites. The DMFT approach applied to this compound yields qualitatively different results compared to those obtained from DFT or DFT+U [33], demonstrating its power in tackling correlated systems with multisite clusters.

Computational tools. To incorporate the electronic and structural degrees of freedom on an equal footing, we employed a state-of-the-art DFT+embedded DMFT code [34,35] which allows relaxation of internal atomic coordinates. In DMFT the experimental lattice

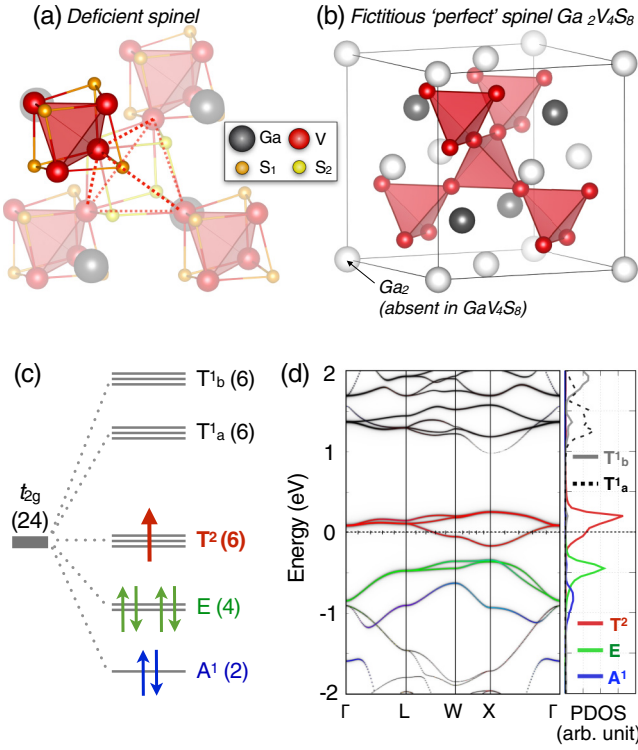


FIG. 1. (a) Crystal structure of the deficient spinel GaV_4S_8 in the cubic phase, in comparison with a fictitious perfect spinel $\text{Ga}_2\text{V}_4\text{S}_8$ illustrated in (b). Note the intercluster V-V bonds depicted in red dashed lines in (a), and white Ga sites in (b) which are absent in deficient spinel structure (a). (c) Splitting of 12 atomic t_{2g} orbitals at 4 V sites in the V_4S_4 cluster into the molecular-orbital (MO) states. Seven electrons in the $(\text{V}_4)^{13+}$ cluster occupy the singlet A^1 , doublet E , and triplet T^2 states, as shown in the diagram. (d) MO-projected fat-band representation and density of state (PDOS) plots of GaV_4S_8 from the DFT results (without U).

parameter reported in Ref. [12] was employed, and optimizations of internal atomic coordinates were done using DMFT forces [36,37]. The hybridization-expansion continuous-time quantum Monte Carlo method [27,28] was employed as the impurity solver. The atomic on-site Coulomb interactions were unitarily transformed and projected onto the MO basis, where the impurity hybridization function has a more appropriate form for the impurity solver [38].

Crystal structure and MO formation. Figure 1(a) shows the crystal structure of cubic GaV_4S_8 . Compared to the fictitious nondeficient spinel $\text{Ga}_2\text{V}_4\text{S}_8$ shown in Fig. 1(b), half of the Ga sites (white Ga_2 sites in the figure) are missing in GaV_4S_8 , which breaks the inversion symmetry (space group $F\bar{4}3m$) and allows the clustering of V and half of S (S_1 sites in the figure). This gives rise to MOs formed out of the 12 atomic t_{2g} orbitals in the V_4 cluster, as depicted in Fig. 1(c), where the 12 orbitals are split into five irreducible representations of the cubic T_d point group, specifically $A^1 \oplus E \oplus T^2 \oplus 2T^1$ (two $2T^1$ denoted as $T^1_{a,b}$ in the diagram). Note that the charge configuration is $(\text{V}_4)^{13+}$, so there are seven electrons left in the cluster, fully occupying the singlet A^1 and doublet E and filling one electron in the T^2 triplet, as shown in Fig. 1(c). The result of a DFT calculation (without including U) is shown

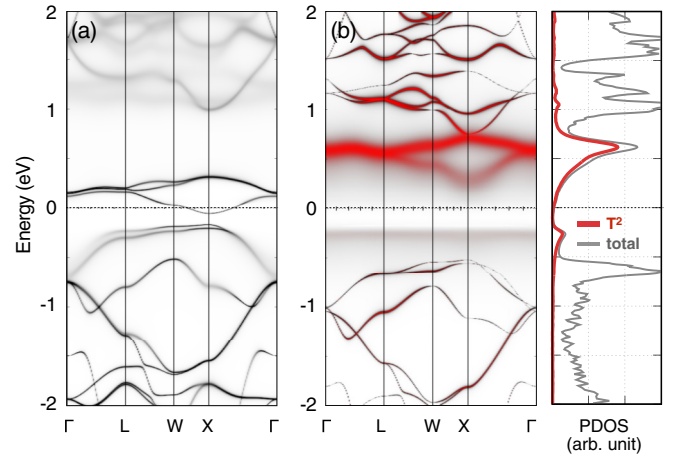


FIG. 2. (a) A plot of the single-site DMFT spectral function with atomic V t_{2g} states chosen as the correlated subspace ($U_d = 6$ eV, $J_H = 0.8$ eV, $T = 232$ K), showing a robust metallic character. (b) MO-DMFT spectral function and PDOS with the MO- T^2 states as the correlated subspace ($U_d = 6$ eV, $T = 232$ K). The red hue in the spectral function plot depicts the character of the MO- T^2 states.

in Fig. 1(d), showing MO-projected fat bands and partial density of states (PDOS) where blue, green, and red colors depict the MO- A^1 , E , and T^2 orbital character, respectively. The MOs can be seen to be well separated in energy and show a narrow bandwidth because of the strong clustering; compared to the size of MO splitting, which is on the order of ~ 1 eV, the magnitude of the intercluster electron hopping is at most ~ 0.02 eV [39]. This implies that the MO orbitals can be a reasonable basis set for the following MO-DMFT calculations.

Single-site vs cluster MO DMFT. Figure 2 shows the comparison between the results from the conventional single-site DMFT and the simplest T^2 -MO-DMFT calculations ($T = 232$ K) [40]. In the latter scheme, one treats the partially filled T^2 triplet MO as the correlated subspace. Note that choosing the T^2 only as the correlated subspace is the simplest cluster-type approximation, but it already yields a completely different result compared to the single-site DMFT. Figure 2(a) shows the k -dependent spectral function from the single-site DMFT calculation, employing the atomic V t_{2g} orbitals as the correlated subspace with an on-site Coulomb repulsion of $U = 6$ eV, appropriate for the V t_{2g} set of quasi-atomic orbitals. A metallic band structure is clearly visible around the Fermi level, similar to the DFT result [Fig. 1(d)], due to the strong hybridization between the intracluster V sites and the mixed valence occupancy ($d^{1.75}$ per V). Increasing the U value within the single-site DMFT did not induce a qualitative change.

While the single-site DMFT cannot open the Mott gap for any physical value of U , the MO-DMFT yields a qualitatively correct result even when applied to the simplest T^2 -triplet MO as shown in Fig. 2(b). Therein the splitting of the T^2 states into the lower and upper Hubbard bands can be seen, depicted in red hue in the spectral function plot (and the red curve in the PDOS), which leads to the opening of a charge gap. Note that since the T^2 triplet is $1/6$ filled, it is not possible to obtain an insulating phase in the band picture

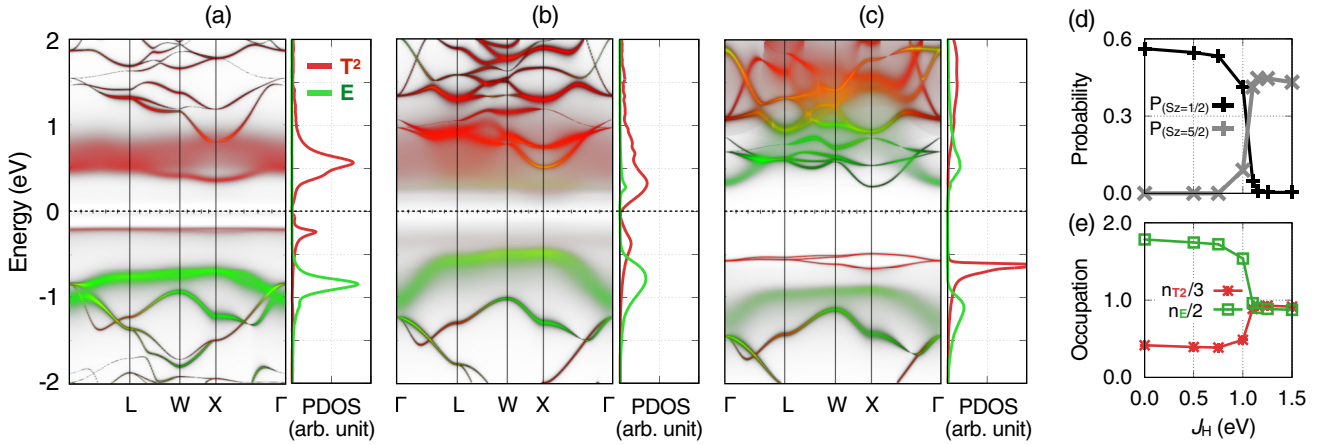


FIG. 3. (a)–(c) Spectral functions and PDOSs with MO- T^2 and E states as correlated subspaces, where the red and green hues depict the T^2 and E characters, respectively. The Hund’s coupling J_H for the correlated $T^2 \oplus E$ subspace is varied from 0 to (a) 0.5 eV, (b) 1.0 eV, and (c) 1.5 eV. Evolution of (d) the probabilities of $S = 1/2$ and $5/2$ configurations and (e) electron occupations in the T^2 (red) and E (green) states as a function of J_H .

without breaking both the cubic and time-reversal symmetries [33], while in the Mott phase both symmetries can be kept. Hence we conclude that the cluster-MO description is indeed crucial in describing the Mott physics of GaV_4S_8 , at least in its cubic and paramagnetic phase. Note that a similar result was previously reported on GaTa_4Se_8 by employing maximally localized Wannier functions for the T^2 triplet and solving the Hubbard model via DMFT [41]. However, as we will show below, this approach overestimates the tendency toward V_4 clustering since it ignores the important effect of the Hund’s coupling between the T^2 and other MOs on the structural degrees of freedom.

$T^2 \oplus E$ subspace and Hund’s coupling. Despite the appearance of the Mott phase within the simplest T^2 -MO-DMFT calculation, this is a crude approximation because other MO states are separated from the T^2 manifold by less than a fraction of an eV, and the Coulomb repulsion as well as the Hund’s coupling are larger or comparable to this separation. Therefore it is important to check what is the effect of including the next set of orbitals into the correlated space. Recently it was shown that the Hund’s coupling can have a very strong effect on the strength of correlations by promoting the local high-spin state and consequently allowing spins to decouple from the orbitals, thus allowing strong orbital differentiation [42–45]. Such physics is completely absent in the T^2 model, as we assumed that the E MOs are completely filled and inert, leaving a single electron in the T^2 MO set.

We next treat the combination of $T^2 \oplus E$ MOs as our correlated subset. Figures 3(a)–3(c) show the orbital-projected spectral functions from calculations with $J_H = 0.5, 1.0,$ and 1.5 eV, respectively ($T = 232$ K, $U = 8$ eV). The red and green colors represent the T^2 and E characters, respectively. The signature of a low-to-high spin crossover, from the $S = 1/2$ to $5/2$ configuration, can be noticed in the plots where the fully occupied E doublet (at $J_H = 0.5$ eV) begins to lose spectral weight as J_H is enhanced. Tracking the Monte Carlo probabilities for the $S_z = 1/2$ and $5/2$ states, plotted in Fig. 3(d), shows the same tendency that the $S_z = 1/2$ probability decreases and collapses almost to zero around

$J_H \sim 1$ eV. Note that we report S_z values rather than S values, because of our choice of an Ising-type approximation of the Coulomb interaction in the MO-DMFT impurity solver [46]. For $J_H \gtrsim 1$ eV, it can be seen that the E doublet becomes half-filled [see Figs. 3(c) and 3(e)], showing that the crossover to the high-spin state is almost complete. Note that even a moderate $J_H \lesssim 1$ eV, appropriate for $3d$ transition-metal compounds [47], induces substantial mixing between the low-spin and high-spin states. Therefore one may suspect a potential role of the Hund’s coupling physics in the high-temperature cubic phase of GaV_4S_8 . Unexpectedly, it turns out that the Hund’s coupling significantly weakens the degree of the V_4S_4 clustering, in contrast with the Coulomb repulsion U which enhances the clustering, as shown in the following.

V_4S_4 clustering from DFT. A parameter quantifying the size of the V_4S_4 clustering is the ratio between the nearest-neighbor V-V distances, $d_{\text{int}}^V/d_{\text{ic}}^V$, where d_{int}^V and d_{ic}^V denote the inter- and intracluster V-V distances, respectively, as shown in Fig. 4(a). $d_{\text{int}}^V/d_{\text{ic}}^V$ is unity in the ideal spinel structure, while in GaV_4S_8 the value was reported to be 1.35 at $T = 295$ K and 1.37 at 20 K, respectively [see the horizontal dashed/dotted lines in Fig. 4(c)] [52].

Figure 4(c) shows the ratios obtained from DFT calculations with different choices of exchange-correlation functionals [30–32,48–51], which have been reported to yield different values of lattice parameters. Three distinct magnetic configurations were considered: a nonmagnetic configuration (NM), a low-spin ferromagnetic configuration (L-FM) with $S = 1/2$, and high-spin ferromagnetic configurations (H-FM) with $S = 5/2$ or $7/2$. These are schematically illustrated in Fig. 4(b). Note that because the V_4 cluster is believed to host a cluster spin moment, FM configurations were considered in our DFT calculations as appropriate for systems with local moments.

Remarkably, the values of $d_{\text{int}}^V/d_{\text{ic}}^V$ shown in Fig. 4(c) are almost identical, at about 1.4, for all the results on the NM or L-FM configurations, despite different optimized lattice parameters (except HSE; see below). Thus, the degree of clustering is consistently overestimated compared to

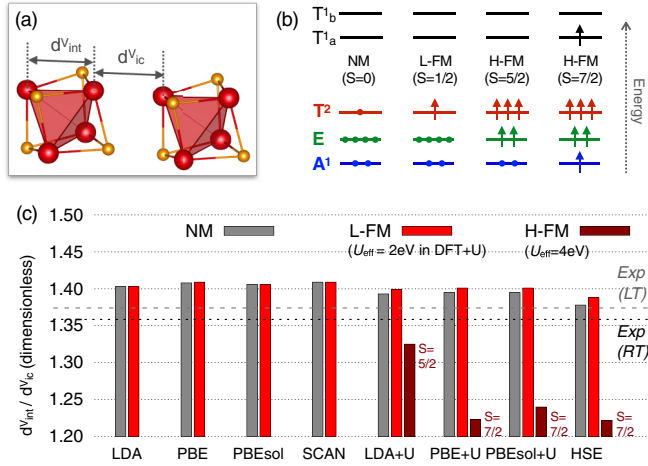


FIG. 4. (a) Definitions of the intra- and intercluster V-V bond lengths d_{int}^V and d_{ic}^V , respectively. (b) Schematic representations of the nonmagnetic (NM), low-spin (L-FM, $S = 1/2$), and high-spin ferromagnetic (H-FM, $S = 5/2$ or $7/2$) configurations, where the dots and arrows depict nonmagnetic and magnetic electrons, respectively. (c) $d_{\text{int}}^V/d_{\text{ic}}^V$ from DFT results with different choices of exchange-correlation potentials: LDA [48], PBE [49], PBEsol [50], SCAN meta-GGA functional [30], DFT+ U [51], and HSE06 hybrid functional [31,32]. In the DFT+ U results, the L-FM and H-FM configurations are obtained by employing $U_{\text{eff}} = 2$ and 4 eV in the simplified rotationally invariant DFT+ U scheme [51]. Horizontal gray dashed and black dotted lines show the values of $d_{\text{int}}^V/d_{\text{ic}}^V$ from experimental structures measured at $T = 295$ and 20 K, respectively [12].

experimental values. On the other hand, the H-FM solutions with the DFT+ U or HSE06 hybrid functionals severely underestimate the clustering, as shown in Fig. 4(c). We notice that in H-FM solutions the lowest occupied MO bonding states (E , A^1) have been emptied at the expense of occupying higher nonbonding- or antibonding-like states. Therefore it is natural that H-FM solutions show a reduced tendency to clustering. Hence it appears that the small but significant discrepancy between the theoretical (in NM or L-FM) and experimental $d_{\text{int}}^V/d_{\text{ic}}^V$ values results from the small admixture of the high-spin configurations to the dominant low-spin configuration in the electronic states of GaV_4S_8 , which cannot be captured in the framework of conventional DFT. Note that even though the HSE06 results with NM or L-FM configurations seem to reproduce reasonable $d_{\text{int}}^V/d_{\text{ic}}^V$ values, those states are much higher in energy by 1.5 eV / f.u. compared to the $S = 7/2$ H-FM phase. Also, all of the DFT results (NM, L-FM, and H-FM) fail to reproduce the insulating phase, signifying the failure of the DFT methods in this system.

$V_4\text{S}_4$ clustering from MO-DMFT. Figure 5 shows the evolution of the $d_{\text{int}}^V/d_{\text{ic}}^V$ values from the DMFT results. As explained above, within the single-site DMFT the correlations appear to be weak, so that the predicted structure is very close to the DFT prediction. As the intracluster correlations are considered via the T^2 MO, the local Hubbard U enhances the clustering tendency, which is clear from the predicted values at $J_H = 0$. It can be seen that the clustering tendency is sub-

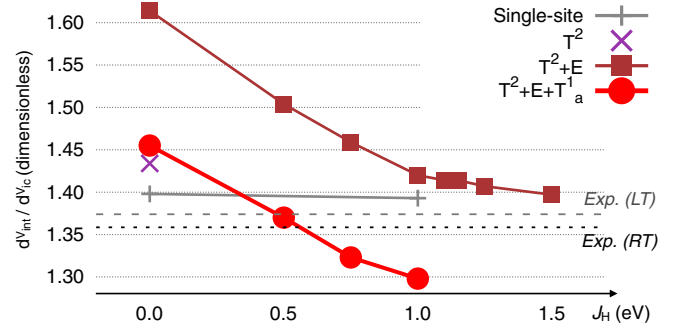


FIG. 5. $d_{\text{int}}^V/d_{\text{ic}}^V$ from DFT results as a function of J_H . Note that MO- T^2 and MO- $\{T^2 \oplus T_a^1\}$ configurations are not affected by J_H because of the single occupancy, and that the MO- $\{T^2 \oplus E \oplus T_a^1\}$ reaches the experimental $d_{\text{int}}^V/d_{\text{ic}}^V$ near $J_H = 0.5$ eV.

stantially overemphasized when the $T^2 \oplus E$ are considered as correlated, due to the bonding nature of the E MO. When the antibonding T_a^1 MO is also included, the degree of clustering reverts back to similar value as for the T^2 -only calculation. Still, the value of $d_{\text{int}}^V/d_{\text{ic}}^V$ is larger than the DFT-optimized one at $J_H = 0$, showing the role of U in enhancing the clustering.

Once the Hund's coupling is turned on, the degree of clustering is quickly reduced (except for the T^2 -only case where there is only one electron) as shown in Fig. 5. We then obtain the experimental $d_{\text{int}}^V/d_{\text{ic}}^V$ values around $J_H = 0.5$ eV, which is a reasonable value for our model, in which e_g states (as well as A^1 and T_b^1) are screening the interaction. This observation is consistent with the spectroscopic tendency mentioned above, where J_H promotes the high-spin state so that spin moments can be more localized on each V site. We thus find, quite surprisingly, that in cases with strong clustering the Coulomb U and Hund's J_H can play opposite roles: the former promotes nonlocal correlations and formation of the bonding molecular orbital state, while the latter promotes local atom-centered high-spin states. This Janus-faced effect of U and J_H is a central result of this study. Note also that the reduction of $d_{\text{int}}^V/d_{\text{ic}}^V$ is significant already at $J_H = 0.5$ eV, where the mixture of the high-spin configurations is quite small as shown in Fig. 3(d). This implies an unusual strong coupling between the electronic configuration and the V_4 clustering, which may be exploited to tune the spin configuration by employing optical pumping techniques as done in VO_2 [53].

Discussion and summary. In summary, in this work we have clarified the significance of electron correlations in describing the MO Mott physics and structural properties of GaV_4S_8 , especially the Janus-faced role of U and J_H in its crystal structure, which can be extended to study the low-temperature ferroelectric and multiferroic phases [20–22] of the same compound and possible unconventional electron-lattice couplings therein. With a careful choice of the MO correlated subspace, our MO-based DMFT approach can tackle systems with large-sized clusters that are not amenable to solution using conventional cluster DMFT approaches, such as $1T\text{-Ta}(\text{S}, \text{Se})_2$ and other cluster Mott-insulating systems [54,55].

Acknowledgments. This work was supported by NSF DMR-1629059. H.-S.K. was funded by the National Research Foundation of Korea (Basic Science Research

Program, Grant No. 2020R1C1C1005900), and also thanks the National Supercomputing Center of Korea for the support

of supercomputing resources including technical assistance (Grant No. KSC-2019-CRE-0036).

- [1] M. H. Whangbo and E. Canadell, Analogies between the concepts of molecular chemistry and solid-state physics concerning structural instabilities. Electronic origin of the structural modulations in layered transition metal dichalcogenides, *J. Am. Chem. Soc.* **114**, 9587 (1992).
- [2] F. J. Morin, Oxides Which Show a Metal-to-Insulator Transition at the Neel Temperature, *Phys. Rev. Lett.* **3**, 34 (1959).
- [3] M. M. Qazilbash, M. Brehm, Byung-Gyu Chae, P.-C. Ho, G. O. Andreev, Bong-Jun Kim, Sun Jin Yun, A. V. Balatsky, M. B. Maple, F. Keilmann, Hyun-Tak Kim, and D. N. Basov, Mott transition in VO₂ revealed by infrared spectroscopy and nano-imaging, *Science* **318**, 1750 (2007).
- [4] S. Biermann, A. Poteryaev, A. I. Lichtenstein, and A. Georges, Dynamical Singlets and Correlation-Assisted Peierls Transition in VO₂, *Phys. Rev. Lett.* **94**, 026404 (2005).
- [5] W. H. Brito, M. C. O. Aguiar, K. Haule, and G. Kotliar, Metal-Insulator Transition in VO₂: A DFT + DMFT Perspective, *Phys. Rev. Lett.* **117**, 056402 (2016).
- [6] J. A. Wilson, F. J. Di Salvo, and S. Mahajan, Charge-density waves and superlattices in the metallic layered transition metal dichalcogenides, *Adv. Phys.* **24**, 117 (1975).
- [7] F. J. Di Salvo and J. E. Graebner, The low temperature electrical properties of 1T-TaS₂, *Solid State Commun.* **23**, 825 (1977).
- [8] P. Fazekas and E. Tosatti, Electrical, structural and magnetic properties of pure and doped 1T-TaS₂, *Philos. Mag. B* **39**, 229 (1979).
- [9] Y. Nakata, K. Sugawara, R. Shimizu, Y. Okada, P. Han, T. Hitosugi, K. Ueno, T. Sato, and T. Takahashi, Monolayer 1T-NbSe₂ as a Mott insulator, *NPG Asia Mater.* **8**, e321 (2016).
- [10] M. Calandra, Phonon-Assisted Magnetic Mott-Insulating State in the Charge Density Wave Phase of Single-Layer 1T-NbSe₂, *Phys. Rev. Lett.* **121**, 026401 (2018).
- [11] H. B. Yaich, J. C. Jegaden, M. Potel, M. Sergent, A. K. Rastogi, and R. Tournier, Nouveaux chalcogénures et chalcobalogénures à clusters tétraédriques Nb₄ ou Ta₄, *J. Less-Common Met.* **102**, 9 (1984).
- [12] R. Pocha, D. Johrendt, and R. Pöttgen, Electronic and structural instabilities in GaV₄S₈ and GaMo₄S₈, *Chem. Mater.* **12**, 2882 (2000).
- [13] R. Pocha, D. Johrendt, B. Ni, and M. M. Abd-Elmeguid, Crystal structures, electronic properties, and pressure-induced superconductivity of the tetrahedral cluster compounds GaNb₄S₈, GaNb₄Se₈, and GaTa₄Se₈, *J. Am. Chem. Soc.* **127**, 8732 (2005).
- [14] D. Johrendt, Crystal and electronic structure of the tetrahedral V₄ cluster compounds GeV₄Q₈ (Q = S, Se), *Z. Anorg. Allg. Chem.* **624**, 952 (1998).
- [15] H. Müller, W. Kockelmann, and D. Johrendt, The magnetic structure and electronic ground states of Mott insulators GeV₄S₈ and GaV₄S₈, *Chem. Mater.* **18**, 2174 (2006).
- [16] H. Chudo, C. Michioka, H. Nakamura, and K. Yoshimura, Magnetic and structural transitions of GeV₄S₈, Proceedings of the International Conference on Strongly Correlated Electron Systems, *Phys. B (Amsterdam, Neth.)* **378-380**, 1150 (2006).
- [17] C. Vaju, J. Martial, E. Janod, B. Corraze, V. Fernandez, and L. Cario, Metal-metal bonding and correlated metallic behavior in the new deficient spinel Ga_{0.87}Ti₄S₈, *Chem. Mater.* **20**, 2382 (2008).
- [18] E. Dorolti, L. Cario, B. Corraze, E. Janod, C. Vaju, H.-J. Koo, E. Kan, and M.-H. Whangbo, Half-metallic ferromagnetism and large negative magnetoresistance in the new lacunar spinel GaTi₃VS₈, *J. Am. Chem. Soc.* **132**, 5704 (2010).
- [19] H.-S. Kim, J. Im, M. J. Han, and H. Jin, Spin-orbital entangled molecular j_{eff} states in lacunar spinel compounds, *Nat. Commun.* **5**, 3988 (2014).
- [20] I. Kézsmárki, S. Bordács, P. Milde, E. Neuber, L. M. Eng, J. S. White, H. M. Rønnow, C. D. Dewhurst, M. Mochizuki, K. Yanai, H. Nakamura, D. Ehlers, V. Tsurkan, and A. Loidl, Néel-type skyrmion lattice with confined orientation in the polar magnetic semiconductor GaV₄S₈, *Nat. Mater.* **14**, 1116 (2015).
- [21] E. Ruff, S. Widmann, P. Lunkenheimer, V. Tsurkan, S. Bordács, I. Kézsmárki, and A. Loidl, Multiferroicity and skyrmions carrying electric polarization in GaV₄S₈, *Sci. Adv.* **1**, e1500916 (2015).
- [22] S. Widmann, E. Ruff, A. Günther, H.-A. Krug von Nidda, P. Lunkenheimer, V. Tsurkan, S. Bordács, I. Kézsmárki, and A. Loidl, On the multiferroic skyrmion-host GaV₄S₈, *Philos. Mag.* **97**, 3428 (2017).
- [23] A. Georges, G. Kotliar, W. Krauth, and M. J. Rozenberg, Dynamical mean-field theory of strongly correlated fermion systems and the limit of infinite dimensions, *Rev. Mod. Phys.* **68**, 13 (1996).
- [24] G. Kotliar, S. Y. Savrasov, K. Haule, V. S. Oudovenko, O. Parcollet, and C. A. Marianetti, Electronic structure calculations with dynamical mean-field theory, *Rev. Mod. Phys.* **78**, 865 (2006).
- [25] K. Held, Electronic structure calculations using dynamical mean field theory, *Adv. Phys.* **56**, 829 (2007).
- [26] G. Kotliar, S. Y. Savrasov, G. Pálsson, and G. Biroli, Cellular Dynamical Mean Field Approach to Strongly Correlated Systems, *Phys. Rev. Lett.* **87**, 186401 (2001).
- [27] K. Haule, Quantum Monte Carlo impurity solver for cluster dynamical mean-field theory and electronic structure calculations with adjustable cluster base, *Phys. Rev. B* **75**, 155113 (2007).
- [28] P. Sémon, Chuck-Hou Yee, Kristjan Haule, and A.-M. S. Tremblay, Lazy skip-lists: An algorithm for fast hybridization-expansion quantum Monte Carlo, *Phys. Rev. B* **90**, 075149 (2014).
- [29] E. Gull, A. J. Millis, A. I. Lichtenstein, A. N. Rubtsov, M. Troyer, and P. Werner, Continuous-time Monte Carlo methods for quantum impurity models, *Rev. Mod. Phys.* **83**, 349 (2011).
- [30] J. Sun, A. Ruzsinszky, and J. P. Perdew, Strongly Constrained and Appropriately Normed Semilocal Density Functional, *Phys. Rev. Lett.* **115**, 036402 (2015).

- [31] J. Heyd, G. E. Scuseria, and M. Ernzerhof, Hybrid functionals based on a screened Coulomb potential, *J. Chem. Phys.* **118**, 8207 (2003).
- [32] J. Heyd, G. E. Scuseria, and M. Ernzerhof, Erratum: Hybrid functionals based on a screened Coulomb potential [J. Chem. Phys. 118, 8207 (2003)], *J. Chem. Phys.* **124**, 219906 (2006).
- [33] M. Sieberer, S. Turnovszky, J. Redinger, and P. Mohn, Importance of cluster distortions in the tetrahedral cluster compounds GaM_4X_8 ($M = \text{Mo}, \text{V}, \text{Nb}, \text{Ta}; X = \text{S}, \text{Se}$): *Ab initio* investigations, *Phys. Rev. B* **76**, 214106 (2007).
- [34] K. Haule, C.-H. Yee, and K. Kim, Dynamical mean-field theory within the full-potential methods: Electronic structure of CeIrIn_5 , CeCoIn_5 , and CeRhIn_5 , *Phys. Rev. B* **81**, 195107 (2010).
- [35] K. Haule, Structural predictions for correlated electron materials using the functional dynamical mean field theory approach, *J. Phys. Soc. Jpn.* **87**, 041005 (2018).
- [36] K. Haule and T. Birol, Free Energy from Stationary Implementation of the DFT + DMFT Functional, *Phys. Rev. Lett.* **115**, 256402 (2015).
- [37] K. Haule and G. L. Pascut, Forces for structural optimizations in correlated materials within a DFT+embedded DMFT functional approach, *Phys. Rev. B* **94**, 195146 (2016).
- [38] Details of this transformation and its implementation in the DFT+embedded DMFT code are discussed in the Supplemental Material. Therein it is argued that intracluster Coulomb repulsions in this system should be insignificant and can be ignored [56]. Note that the DFT+embedded DMFT code runs based on the WIEN2K package [57]. Choices of U and J values in this DMFT implementation was discussed in Ref. [58]. The Vienna *Ab initio* Simulation Package (VASP) [59, 60] was used for independent structural optimizations at the DFT level.
- [39] A. Camjayi, R. Weht, and M. J. Rozenberg, Localised Wannier orbital basis for the Mott insulators GaV_4S_8 and GaTa_4Se_8 , *Europhys. Lett.* **100**, 57004 (2012).
- [40] See Supplemental Material at <http://link.aps.org/supplemental/10.1103/PhysRevB.102.081105> for the details of the single-site DMFT.
- [41] A. Camjayi, C. Acha, R. Weht, M. G. Rodríguez, B. Corraze, E. Janod, L. Cario, and M. J. Rozenberg, First-Order Insulator-to-Metal Mott Transition in the Paramagnetic 3D System GaTa_4Se_8 , *Phys. Rev. Lett.* **113**, 086404 (2014).
- [42] K. Haule and G. Kotliar, Coherence-incoherence crossover in the normal state of iron oxypnictides and importance of Hund's rule coupling, *New J. Phys.* **11**, 025021 (2009).
- [43] Z. P. Yin, K. Haule, and G. Kotliar, Kinetic frustration and the nature of the magnetic and paramagnetic states in iron pnictides and iron chalcogenides, *Nat. Mater.* **10**, 932 (2011).
- [44] Z. P. Yin, K. Haule, and G. Kotliar, Fractional power-law behavior and its origin in iron-chalcogenide and ruthenate superconductors: Insights from first-principles calculations, *Phys. Rev. B* **86**, 195141 (2012).
- [45] A. Georges, L. de' Medici, and J. Mravlje, Strong correlations from Hund's coupling, *Annu. Rev. Condens. Matter Phys.* **4**, 137 (2013).
- [46] This approximation leads to some mixing between half-integer spin states, but is not expected to change qualitative aspects of the results .
- [47] L. Vaugier, H. Jiang, and S. Biermann, Hubbard U and Hund exchange J in transition metal oxides: Screening versus localization trends from constrained random phase approximation, *Phys. Rev. B* **86**, 165105 (2012).
- [48] D. M. Ceperley and B. J. Alder, Ground State of the Electron Gas by a Stochastic Method, *Phys. Rev. Lett.* **45**, 566 (1980).
- [49] J. P. Perdew, K. Burke, and M. Ernzerhof, Generalized Gradient Approximation Made Simple, *Phys. Rev. Lett.* **77**, 3865 (1996).
- [50] G. I. Csonka, J. P. Perdew, A. Ruzsinszky, P. H. T. Philipsen, S. Lebègue, J. Paier, O. A. Vydrov, and J. G. Ángyán, Assessing the performance of recent density functionals for bulk solids, *Phys. Rev. B* **79**, 155107 (2009).
- [51] S. L. Dudarev, G. A. Botton, S. Y. Savrasov, C. J. Humphreys, and A. P. Sutton, Electron-energy-loss spectra and the structural stability of nickel oxide: An LSDA+U study, *Phys. Rev. B* **57**, 1505 (1998).
- [52] Note that at $T = 20\text{K}$, the compound has a rhombohedral distortion. The value 1.37 is obtained by averaging d_{int}^V and d_{ic}^V separately and taking the ratio between them.
- [53] Z. Yang, C. Ko, and S. Ramanathan, Oxide electronics utilizing ultrafast metal-insulator transitions, *Annu. Rev. Mater. Res.* **41**, 337 (2011).
- [54] G. Chen, H.-Y. Kee, and Y. B. Kim, Fractionalized Charge Excitations in a Spin Liquid on Partially Filled Pyrochlore Lattices, *Phys. Rev. Lett.* **113**, 197202 (2014).
- [55] G. Chen and P. A. Lee, Emergent orbitals in the cluster Mott insulator on a breathing kagome lattice, *Phys. Rev. B* **97**, 035124 (2018).
- [56] K. Haule, Exact Double Counting in Combining the Dynamical Mean Field Theory and the Density Functional Theory, *Phys. Rev. Lett.* **115**, 196403 (2015).
- [57] P. Blaha, K. Schwarz, G. K. H. Madsen, D. Kvasnicka, and J. Luitz, *WIEN2k, An Augmented Plane Wave + Local Orbitals Program for Calculating Crystal Properties* (Karlheinz Schwarz, Techn. Universität Wien, Austria, 2001).
- [58] K. Haule, T. Birol, and G. Kotliar, Covalency in transition-metal oxides within all-electron dynamical mean-field theory, *Phys. Rev. B* **90**, 075136 (2014).
- [59] G. Kresse and J. Hafner, *Ab initio* molecular dynamics for liquid metals, *Phys. Rev. B* **47**, 558 (1993).
- [60] G. Kresse and J. Furthmüller, Efficient iterative schemes for *ab initio* total-energy calculations using a plane-wave basis set, *Phys. Rev. B* **54**, 11169 (1996).